Evidence for Bosonization in a three-dimensional gas of SU(N) fermions

Bo Song,^{1,*} Yangqian Yan,^{2,*} Chengdong He,¹ Zejian Ren,¹ Qi Zhou,^{2,3,†} and Gyu-Boong Jo^{1,‡}

¹Department of Physics, The Hong Kong University of Science and Technology,

Clear Water Bay, Kowloon, Hong Kong, China

²Department of Physics and Astronomy, Purdue University, West Lafayette, Indiana 47907, USA

³ Purdue Quantum Science and Engineering Institute, Purdue University,

1205 W State St, West Lafayette, West Lafayette, IN 47907, USA

(Dated: June 27, 2022)

A multi-component Fermi gas with SU(N) symmetry is expected to behave like spinless bosons in the large N limit, where the large number of internal states weakens constraints from the Pauli exclusion principle [1]. Whereas blurring the boundary between bosons and fermions lies at the heart of multiple disciplines [2-5], bosonization of SU(N) fermions has been experimentally tested only in a one-dimensional (1D) system so far [6]. Here, we report evidence for bosonization in a three-dimensional (3D) SU(N) fermionic Ytterbium gas with tunable N. Using the column integrated momentum distribution, we measure contacts, the central quantity controlling dilute quantum gases [7–9], with a high signal-to-noise ratio in our system. We find that the contact per spin approaches a constant with a 1/N scaling in the low fugacity regime. This scaling signifies the vanishing role of the fermionic statistics in thermodynamics, and unfolds the intriguing nature of bosonization in 3D SU(N) fermions. Our work suggests a new route of using contacts to explore multi-component quantum systems and their underlying symmetries.

Bosons and fermions exhibit intrinsically different properties because of the distinct underlying statistics. Strikingly, the boundary between bosons and fermions could become blurred under a variety of scenarios, ranging from the supersymmetry exchanging bosons and fermions to fermionization of strongly interacting bosons in 1D [2, 3]. In the latter case, hardcore bosons and noninteracting fermions share identical thermodynamical properties despite that their correlation functions are different. With increasing N in SU(N) fermions, the Pauli exclusion principle becomes less effective in determining thermodynamical properties of a many-body system [1]. Whereas this mechanism seems independent on the dimensionality of the system, bosonization of SU(N)fermions have only be observed so far in 1D based on the measurement of the breathing mode [6].

In this work, we explore bosonization of a 3D SU(N) fermion gas by measuring its central quantity, the socalled contacts, C [7–9]. Through celebrated universal relations, contacts govern many other physical observables, such as the momentum distribution, the energy, the pressure, and a variety of spectroscopies [7–9]. Therefore, the dependence of contacts on N directly provides us with the evidence of bosonization without resorting measuring other thermodynamical quantities. We choose $^{173}{\rm Yb}$ atoms as our sample, in which the number of internal states accessible in experiments is highly tunable, ranging from one to six. Due to the strong decoupling between electronic and nuclear spins, interactions between nuclear spins are isotropic, providing the many-body system with a ${\rm SU}(N)$ symmetry and consequently, a wide range of exotic phenomena [10–13].

Whereas the SU(N) symmetry has been explored in optical lattices [6, 14–16], a spectroscopy [17], and collective excitations [6, 18], it is challenging to measure the rather small contact due to the weak interactions between ¹⁷³Yb atoms. To overcome this obstacle, we develop a new protocol to extract the contact from the column integrated momentum distribution without using the inverse-Abel transform, which allows a high signal-tonoise ratio (SNR). We observe that the contact increases as $(T/T_F)^{-3/2}$, when the temperature T/T_F decreases from $T/T_F=1.0$ to 0.55. When N is fixed, no change in the measured contact is observed for different spin constituents, confirming the isotropic interaction. We further change the number of nuclear spin component Nand keep the number of atoms per component constant at the same temperature and trap geometry. We find a linear dependence of the contact with N. Consequently, the contact per spin approaches a constant with increasing N.

The observed scalings of contacts can be qualitatively understood as follows. As depicted in Fig.1, in a balanced SU(N) gas with N_0 atoms per spin state, a single atom with spin- σ interacts with $(N-1)N_0$ atoms in the other (N-1) spin components with spin- σ' $(\sigma' \neq \sigma)$ through the s-wave scattering. When interactions are spin-independent, each pair of atoms contributes an equal amount, c_{pair} , to the large momentum tail, $n_{3D}^{\sigma}(\vec{k}) = C_0/k_{3D}^4$, where $\vec{k} = (k_x, k_y, k_z)$ is a 3D momentum vector and $k_{3D} = |\vec{k}|$ is much larger than k_F and other microscopic momentum scales. In the low fugacity regime where three-body correlations are negligible, $C_0 = c_{\text{pair}}(N-1)N_0^2$, i.e., scaled with (N-1) when the number of spin, N, is tuned. Correspondingly, if we consider the total momentum distribution,

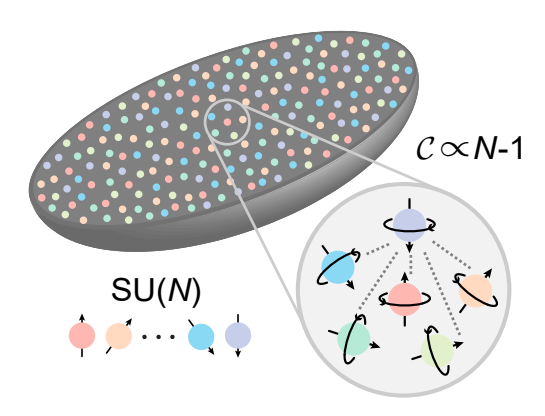


Figure 1: Illustration of s-wave contacts in SU(N) fermions with tunable spin. Arrows with different colors and orientations denote the different nuclear spin states as large as N=6. Dashed lines represent pairs formed by two particles with different spins. Each pair contribute the same amount to the contact such that $C \sim N-1$.

 $n_{3D}(\vec{k}) = \sum_{\sigma} n_{3D}^{\sigma}(\vec{k})$, we could define the total contact, $C_{\mathrm{SU(N)}} = NC_0 = c_{\mathrm{pair}}N(N-1)N_0^2$. Dividing $C_{\mathrm{SU(N)}}$ by N_t^2 , where $N_t = NN_0$ is the total particle number, we obtain that $C_{\mathrm{SU(N)}}/N_t^2 = c_{\mathrm{pair}}(1-1/N)$.

In our experiment, p-wave contacts [19] are expected to be negligible, as the current temperature regime is smaller than the barrier of the p-wave interaction [20]. We, therefore, treat SU(1) fermions as non-interacting systems. This is precisely the origin of the 1/N factor in the scaling of $C_{SU(N)}/N_t^2$ with N. The Pauli exclusion principle suppresses the s-wave scattering between two atoms with the same spin, as well as their contributions to the s-wave contact. To have a comparison, we consider spinless bosons with the same N_t , T and the same scattering length, a_s . Though c_{pair} is independent on statistics, all $N_t(N_t-1)/2$ pairs of particles in spinless bosons contribute to contacts such that the high momentum tail is written as $n_{\rm B}(\vec{k}) = C_{\rm B}/k_{\rm 3D}^4$, where $C_{\rm B} = c_{\rm pair} N_t (N_t - 1) \approx c_{\rm pair} N_t^2$ for large N_0 , as the momentum distribution of identical particles doubles that of distinguishable particles. We obtain $\mathcal{C}_{SU(N)}/N_t^2 =$ $C_{\rm B}/N_t^2(1-1/N)$, which shows that the s-wave contact of SU(N) fermions approaches that of bosons with a 1/Nscaling. Since $C_0/N = (C_{SU(N)}/N_t^2)N_0^2$, we use the contact per spin, C_0/N , to capture this scaling with a fixed N_0 .

The experiment starts with degenerate fermions prepared in a crossed hybrid optical dipole trap (ODT) consisting of far-detuned 1064 nm and 532 nm laser light. A six-component Fermi gas of 173 Yb atoms, loaded from an inter-combination magneto-optical trap, is evaporatively cooled down to the temperature ~ 100 nK in the ODT in 6s. Along with the evaporation, an arbitrary spin mixture with N=1,2,...,6 is prepared by the use of optical pumping and blasting processes [21]. Next, we exponen-

tially ramp up ODT trap to the final trap depth within 60 ms resulting in sufficiently large trap frequencies (see Methods for details). Finally, the momentum distribution after a 4ms time-of-flight expansion is recorded in the k_x - k_y plane by absorption imaging along the z direction using the resonant imaging light of ${}^1S_0 \rightarrow {}^1P_1$ transition. In Fig. 2(b), a typical high-momentum tail is observed in the $\mathcal S$ profile after the systematic noise is filtered out [22].

Our schematic protocol, for the high-precision measurement of the contact, is based on the momentum distribution of the atomic cloud after the time-of-flight expansion as shown in Fig.2. Typically, to measure contacts from the momentum distribution, the atomic profile recorded in the 2D plane, which represents the column integrated momentum distribution, needs to be inverse-Abel transformed to 3D momentum distribution. However, inverse-Abel transform often intensifies measurement noise and exacerbates SNR because it involves a derivative of the atomic distribution, which inevitably limits our capability to detect contacts in a weakly interacting SU(N) Fermi gas. To overcome this limitation, we extract contacts directly based on the weight of the highmomentum tail from a 2D time-of-flight image without using the inverse-Abel transform.

When k_{3D} is much larger than the inverse of the harmonic oscillator length and other microscopic momentum scales, $n_{3D}^{\sigma}(\vec{k})$ becomes isotropic in 3D and follows a scaling law, $n_{3D}^{\sigma}(k_{3D}) \to \mathcal{C}_0/k_{3D}^4$ where $n_{3D}^{\sigma}(k_{3D})$ is the atom number at k_{3D} . Here, we have used \mathcal{C}_0 to distinguish the original definition of contact from the scaled one, C, used in our experiment. To be noted, in a spinbalanced Fermi gas with N components, atom density for each spin $n_{3D}^{\sigma}(k_{3D})$ is identical. Hereafter, it is normalized such that $\int n_{3D}^{\sigma}(k_{3D})d^3k_{3D} = 1$ in our experiment. Correspondingly, the column integrated momentum distribution, $n^{\sigma}(k) = \int_{-\infty}^{\infty} n_{3D}^{\sigma}(k_{3D}) dk_z$, which follows $\int n^{\sigma}(k)2\pi k dk = 1$. The momentum is normalized by the Fermi wave number $k_F = \sqrt{2E_F m}/\hbar$ with the Fermi energy $E_F = \hbar \bar{\omega} (6N_0)^{1/3}$. Here $\bar{\omega}$ is the averaged trap frequency, m is the mass of $^{173}\mathrm{Yb}$ and \hbar is the reduced Planck constant. Contact C can be experimentally extracted from the high momentum plateau of a term $S = 2/\pi \cdot k^3 n^{\sigma}(k)$ as follows (see Methods),

$$C = \lim_{k \to \infty} S(k) = \lim_{k \to \infty} \frac{2}{\pi} \cdot k^3 n^{\sigma}(k) = \frac{C_0}{(2\pi)^3 N_0 k_F}.$$
 (1)

Here, \mathcal{C} is naturally normalized by the atom number per spin N_0 and the Fermi wave number k_F . The key advantage of our protocol is that no transform gets involved resulting a high SNR ratio. To further diminish the noise of the atomic profile, we typically repeat the measurement ~ 100 times and obtain an averaged image as shown in Fig.2(a), and then azimuthally average the momentum distribution profile with $\pm 0.2k_F$ moving average.

Because of the small scattering length of 173 Yb, contacts in our SU(N) gas are contained in the large mo-

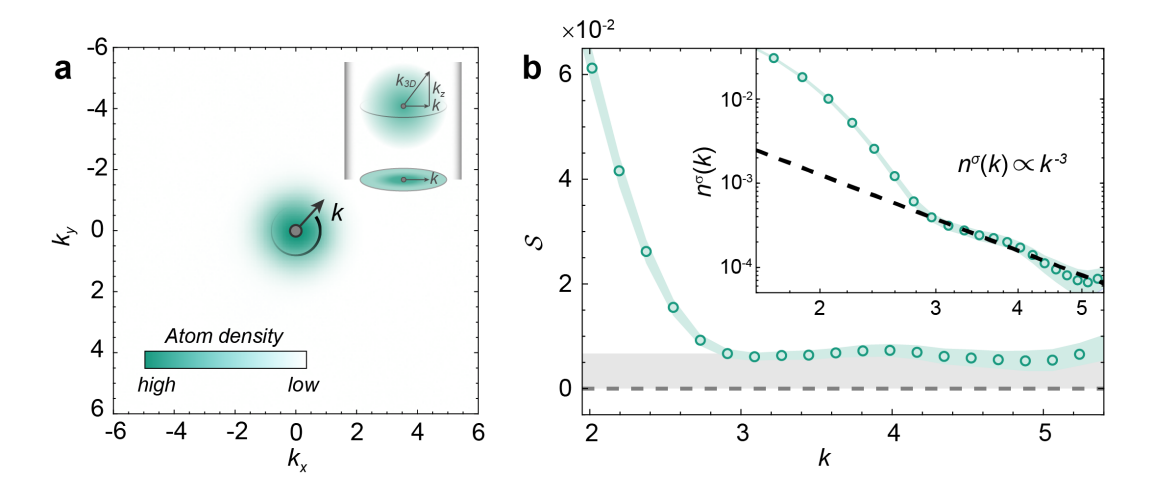


Figure 2: Measurement of the contact parameter from the momentum distribution. (a) momentum distribution of 173 Yb atoms consisting N=6 nuclear spin states after 4 ms time-of-flight expansion. Momentum here is normalized by the Fermi wave number k_F . Note that momentum profile outside $k \simeq 2.5$ has already been subtracted by the momentum profile of the spin-polarised gas (N=1) with the same atom number. (b) the term $\mathcal{S}=2/\pi \cdot k^3 n^{\sigma}(k)$ is plotted as a function of momentum k in units of k_F . Inset is the momentum tail of azimuthally averaged atomic distribution $n^{\sigma}(k)$ in logarithmic scale with a dashed guideline of $n^{\sigma}(k) \propto k^{-3}$. The $n^{\sigma}(k)$ is normalized as $\int n^{\sigma}(k) 2\pi k dk = 1$. The finite value of the contact is determined from the plateau of the \mathcal{S} profile in the range of k=3 to 4. The green shaded area stands for the experimental uncertainty.

mentum tail with an extremely small amplitude that is below a thousandth of the maximum cloud density. To extract such high-momentum tail from the subtle density profile, we first filter out the systematic noise (e.g. interference fringes, imaging light fluctuation) using the statistical method. Our protocol is based on statistical image decomposition and projection methods using the data images as a basis set and compensating for unwanted fringes [22]. Secondly, we compare the high-momentum tail of SU(N > 1) fermions with respect to non-interacting SU(1) gases, and extract the highmomentum tail of SU(N > 1) gases after subtracting the counterpart of SU(1). This allows us to systematically eliminate the diffraction effect arising from atoms. Note that for a SU(1) gas, we first separate the data set of SU(1) into two parts and analyse them using a similar procedure.

In Fig. 3, we show the measured \mathcal{C} at temperatures between $T/T_F = 0.55$ and $T/T_F = 1$ for SU(N=1,3,6). We change the number of components, N=1,2,...,6, but keep the same number of atoms per spin component $N_0=6.7\times10^3$ in a 3D harmonic trap with frequencies $(\omega_x,\omega_y,\omega_z)=2\pi\times(1400,750,250)$ Hz and the averaged trap frequency $\bar{\omega}=(\omega_x\omega_y\omega_z)^{1/3}=2\pi\times640$ Hz. We post-select data images based on the atom number and temperature with tolerance of $\sim 0.1T_F$. As expected, a spin-polarized SU(1) gas with negligible p-wave scatterings does not exhibit k^4 momentum tail within our experimental uncertainty while the finite contact is clearly observed for a SU(6) or SU(3) Fermi gas in Fig. 3(a). Within the temperature regime we explored, the contact increases as

the temperature T/T_F decreases.

In Fig. 4, we test the scaling of the contact with the number of the spin components in SU(N) Fermi gases. We first collapse data points in Fig. 3(a) to the Fermi temperature using $\mathcal{C} \propto (T/T_F)^{-3/2}$ shown in Fig. 3(b). The results clearly show that \mathcal{C} scales with $(T/T_F)^{-3/2}$. We further explore the dependence of the contact on N. Fig. 4(a) shows that \mathcal{C} depends linearly on (N-1), and Fig. 4(b) demonstrates that $\mathcal{C}/N \sim \mathcal{C}_0/N$ approaches a constant with a 1/N scaling. All results are consistent with the qualitative picture we previously provided.

To measure $n^{\sigma}(k)$, we need to release atoms from the trap. Due to the absence of Feshbach resonance, interactions here cannot be turned off, unlike ⁴⁰K for studying s-wave contacts of two-component fermions [23]. Interactions lead to complex expansion dynamics that are difficult to compute in theory. Therefore, it is illuminating to theoretically study contacts of trapped gases before the expansion. We compute contacts in the temperature regime explored in the experiments, $0.55 < T/T_F < 1.0$, where the second order virial expansion works well and high order virial expansion are negligible [24, 25]. We evaluate the local contact at the position \vec{r} based on its local chemical potential $\mu_{loc} = \mu_0 - V(\vec{r})$, where μ_0 is the chemical potential at the center of the trap and $V(\vec{r})$ is the harmonic trapping potential. The total contact is obtained by integrating local contacts in the trap. The total contact per spin state is written as $\mathcal{C}_0 =$ $k_B T \frac{8\pi m}{\hbar^2} (\frac{k_B T}{\hbar \omega})^3 z^2 \frac{a_s^2}{2^{3/2} \lambda} (N-1)$. $\lambda = \sqrt{2\pi \hbar^2/(mk_B T)}$ is the thermal wavelength, and $z = e^{\beta \mu_{loc}}$ is the fugacity. In this temperature regime, the chemical potential μ_0 is well

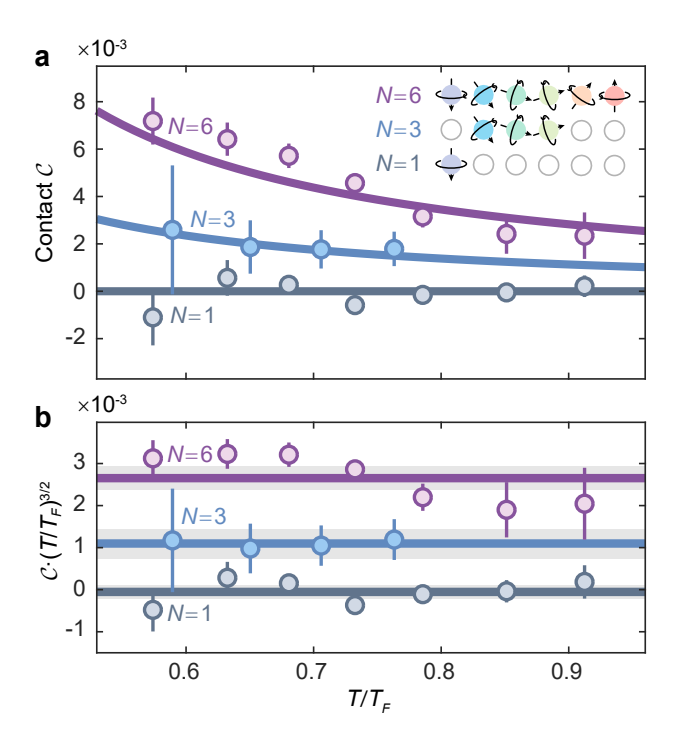


Figure 3: Temperature scaling of contacts in SU(N) fermions. (a) Contact is measured at different temperature in the SU(N) Fermi gases. The error bars represent one standard deviation in the plateau area of S profile. The solid curves are theoretical results multiplied by a factor of 6.5. Spin configuration of different SU(N) gases are presented by arrows in spheres and the circle with empty inside indicates the absence of the spin state. Details of spin configurations and preparation of different SU(N) gases are described in Methods. The result shows a good agreement with the temperature scaling $\mathcal{C} \propto (T/T_F)^{-3/2}$. (b) Using the temperature scaling $\mathcal{C} \propto (T/T_F)^{-3/2}$, contacts of SU(N) gases at different temperature are collapsed to the Fermi temperature $T=T_F$. The solid line are means of collapsed contacts. The shaded grey area indicates the experimental uncertainty which consists of the standard error and the standard deviation of each point.

approximated by $\mu_0 = -T/T_F \cdot \log(6(T/T_F)^3)E_F$ [26]. We obtain

$$C = \frac{C_0}{(2\pi)^3 N_0 k_F} \approx \frac{ma_s^2}{6(2\pi)^{5/2} \hbar^2} \frac{E_F}{(T/T_F)^{3/2}} (N-1). \quad (2)$$

We observe that C scales with N-1 and $(T/T_F)^{-3/2}$ in the high temperature regime. Both scalings are consistent with the aforementioned experimental results, suggesting that interactions during the expansion do not change the scalings of the contact with T and N.

Using the virial expansion, the s-wave contact of spinless boson is also obtained explicitly in the same low fugacity regime (see Methods). We then find

$$C_{SU(N)} = NC_0 = \left(1 - \frac{1}{N}\right)C_B.$$
 (3)

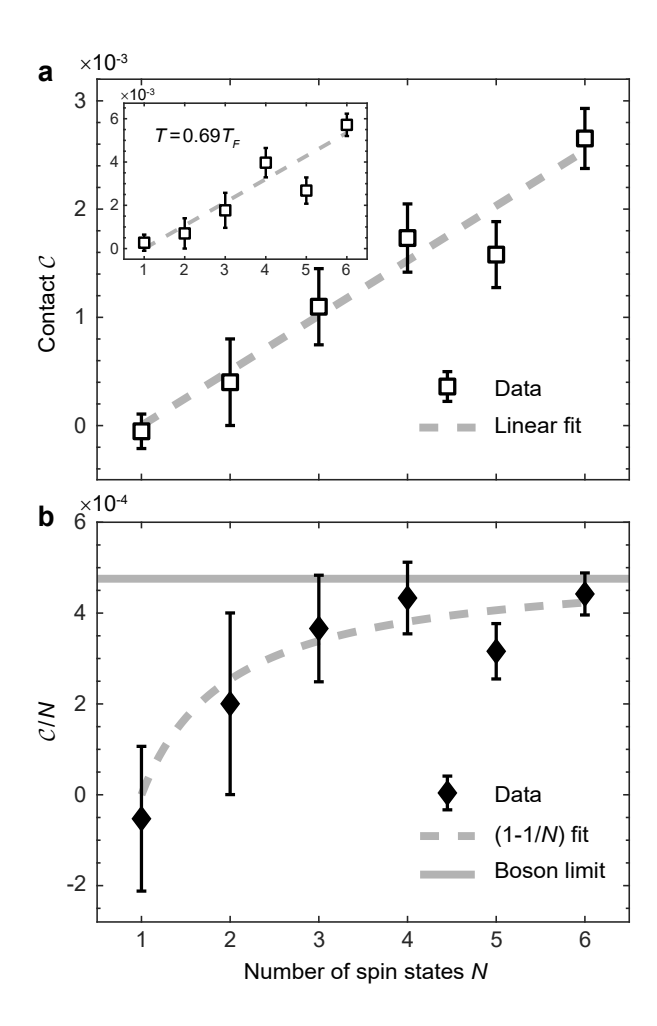


Figure 4: Scaling of the contact in SU(N) fermions with tunable spin. (a) Contacts scale linearly with the number of spin components in a SU(N) Fermi gas. Mean values of collapsed contacts at $T=T_F$ of SU(N) gases are plotted as a function of number of spin states. The dashed line is a linear fit to (N-1). Inset shows the contact at $T=0.69T_F$. (b) Contact per spin, \mathcal{C}/N , as a function of N. The dashed line indicates a (1-1/N) fit to the data. The horizontal solid line denotes the theoretical result of trapped bosons, $N_0\mathcal{C}_{\rm B}/(8\pi^3k_FN_t^2)$, multiplied by 6.5.

As contact is the central quantity to control the manybody system, Eq.(3) is a direct proof of the bosonization without resorting to any other quantities, such as the full momentum distribution.

Whereas scalings of the measured contacts with N and T after the expansion are consistent with theoretical results of trapped gases, experimental results lie systematically above theoretical ones, the former about 6.5 times larger than the latter (see Methods). It is interesting to note that such discrepancy was also observed in an experiment measuring contacts of a weakly interacting Bose-Einstein condensate of Helium-4 atoms [27]. Interactions remain finite during expansions in both cases. It is, therefore, possible that interaction effects during

the expansion lead to the aforementioned discrepancy. However, the current resolution limits our capability to measure the time dependence of contacts in the expansion, which by itself is an interesting question concerning the non-equilibrium dynamics of contacts. To avoid this issue and directly access contacts of trapped gases, an alternative scheme is the Bragg spectroscopy without the expansion [28].

We have focused on the low fugacity regime. With decreasing T, higher order virial expansions will become important. Though bosonization still exists, scalings with T and N are expected to change. It is desirable to study how the difference between contacts of $\mathrm{SU}(N)$ fermions and spinless bosons scales with some powers of 1/N. With further decreasing T down to below the superfluid transition temperature, our scheme of measuring contacts without using the inverse-Abel transform will provide us with an even richer playground to study contacts of superfluids with the $\mathrm{SU}(N)$ symmetry. It is also generically applicable to other atomic systems including bosons.

- * These authors contributed equally to this work.
- † Electronic address: zhou753@purdue.edu
- [‡] Electronic address: gbjo@ust.hk
- C. N. Yang and Y. Yi-Zhuang, Chinese Physics Letters 28, (2011).
- [2] S. Weinberg, *The Quantum Theory of Fields* (The Quantum Theory of Fields, University of Texas, Austin, 2000).
- [3] T. Giamarchi, Quantum Physics in One Dimension (Clarendon Press, 2003).
- [4] Z. X. Li, A. Vaezi, C. B. Mendl and H. Yao, Science advances 4, eaau1463 (2018).
- [5] A. Cherman and D. Dorigoni, Journal of High Energy Physics 2012, 173 (2012).
- [6] G. Pagano, M. Mancini, G. Cappellini, P. Lombardi, F. Schäfer, H. Hu, X.-J. Liu, J. Catani, C. Sias, M. Inguscio et al., *Nature Physics* 10, 198 (2014).
- [7] S. Tan, Annals of Physics 323, 2952 (2008).
- [8] S. Tan, Annals of Physics **323**, 2971 (2008).
- [9] S. Tan, Annals of Physics **323**, 2987 (2008).
- [10] C. Wu, J.-p. Hu and S.-C. Zhang, Physical Review Letters 91, 186402 (2003).
- [11] M. Hermele, V. Gurarie and A. Rey, Physical Review Letters 103, 135301 (2009).
- [12] A. V. Gorshkov, M. Hermele, V. Gurarie, C. Xu, P. S. Julienne, J. Ye, P. Zoller, E. Demler, M. D. Lukin and A. M. Rey, *Nature Physics* 6, 289 (2010).
- [13] M. A. Cazalilla and A. M. Rey, Reports on Progress in Physics 77, 124401 (2014).
- [14]S. Taie, R. Yamazaki, S. Sugawa and Y. Takahashi, $Nat.Phys~\mathbf{8},~825$ (2012).
- [15] C. Hofrichter, L. Riegger, F. Scazza, M. Höfer, D. R. Fernandes, I. Bloch and S. Fölling, *Physical Review X* 6, 021030 (2016).
- [16] H. Ozawa, S. Taie, Y. Takasu and Y. Takahashi, Physical Review Letters 121, 225303 (2018).

- [17] X. Zhang, M. Bishof, S. L. Bromley, C. V. Kraus, M. S. Safronova, P. Zoller, A. M. Rey and J. Ye, *Science* 345, 1467 (2014).
- [18] C. He, Z. Ren, B. Song, E. Zhao, J. Lee, Y.-C. Zhang, S. Zhang and G.-B. Jo, arXiv.org 345, (2019).
- [19] C. Luciuk, S. Trotzky, S. Smale, Z. Yu, S. Zhang and J. H. Thywissen, *Nature Physics* 12, 599 (2016).
- [20] T. Fukuhara, Y. Takasu, M. Kumakura and Y. Takahashi, *Physical Review Letters* 98, 030401 (2007).
- [21] B. Song, C. He, S. Zhang, E. Hajiyev, W. Huang, X.-J. Liu and G.-B. Jo, *Physical Review A* **94**, 061604 (2016).
- [22] In preparation **94**, (2019).
- [23] J. T. Stewart, J. P. Gaebler, T. E. Drake and D. S. Jin, Physical Review Letters 104, 235301 (2010).
- [24] H. Hu, X.-J. Liu and P. D. Drummond, New Journal of Physics 13, 035007 (2011).
- [25] M. Sun and X. Leyronas, Physical Review A (Atomic, Molecular, and Optical Physics) 92, 775 (2015).
- [26] D. Butts and D. Rokhsar, *Physical Review A* 55, 4346 (1997).
- [27] R. Chang, Q. Bouton, H. Cayla, C. Qu, A. Aspect, C. I. Westbrook and D. Clément, *Physical Review Letters* 117, 235303 (2016).
- [28] C. Carcy, S. Hoinka, M. G. Lingham, P. Dyke, C. C. N. Kuhn, H. Hu and C. Vale, *Physical Review Letters* 122, 203401 (2019).
- [29] X.-J. Liu, Physics Reports **524**, 37 (2013).
- [30] S. E. Gharashi, K. Daily and D. Blume, *Physical Review A* 86, 042702 (2012).
- [31] T. Busch, B. G. Englert, K. Rzazewski, and M. Wilkens, Foundations of Physics 28 549-559 (1998).
- [32] T.-L. Ho and E. J. Mueller, Physical review letters 92, 160404 (2004).

Methods

Preparation of SU(N) gases SU(N) symmetric interaction in the ground state $^{1}\text{S}_{0}$ of ^{173}Yb atoms emerges from the decoupling between nuclear spin and orbital angular momentum (J=0). Exploiting the energy splitting of the excited state in $^{3}\text{P}_{1}$ to our advantage, the narrow line-width transition $^{1}\text{S}_{0}(F=5/2) \rightarrow ^{3}\text{P}_{1}(F'=7/2)$, with wavelength $\lambda=556$ nm and natural line-width $\Gamma=2\pi\times181$ kHz, is used as a blasting light to remove unwanted m_{F} states of the ground manifold $^{1}\text{S}_{0}$.

The preparation starts with a gas of spin-balanced six m_F states which is initially loaded in an optical dipole trap. A sequence of short pulses of σ^{\pm} optical blasting light resonance to transition $m_F \to m_F \pm 1$, is applied after the end of the evaporative cooling, where the temperature of atoms is $T\sim100$ nK. The magnetic field of 13.6 G is applied leading to a Zeeman splitting of 8.4 MHz \sim 46 Γ between two adjacent m_F states in the ³P₁ state. Take the preparation of a spin-balanced SU(2) gas as an example, we shine pulses of resonant blasting light with transitions $m_F = 1/2 \rightarrow m_F' = 3/2$, $m_F = 3/2 \rightarrow m_F' = 5/2$ with σ^+ polarization to remove positive $m_F = 1/2$ and $m_F = 3/2$ respectively, and $m_F = -1/2 \rightarrow m_F' = -3/2, m_F = -3/2 \rightarrow m_F' = -5/2$ with σ^- polarization to remove negative $m_F = -1/2$ and $m_F = -3/2$ respectively, and the duration of each pulse is 5 ms. Following the similar method, arbitrary spin configuration of the SU(N) (N=1,2...,6) gas can be prepared by the combination of σ^+ and σ^- lights. The spin configurations of different SU(N) gases used in the experiment are detected by optical Stern Gerlach effect [21] as shown in Fig. M1.

Notably, we use optical pumping to prepare spin polarized gases (N=1) with different atom numbers. At the beginning of evaporation, we first optically pump most the atoms to the $m_F=5/2$ state using another optical pumping light 400 MHz red detuned from the resonance with $^1{\rm S}_0 \rightarrow ^1{\rm P}_1$ transition. The pumping pulse time is 300 ms. Note that we intentionally leave other spin states for the sake of the evaporative cooling. At the end of the evaporation, all the other remained spin states are removed by 556nm resonance light pulses similar to the procedure of ${\rm SU}(N)$ gas preparation.

We further increase the trap depth to obtain large trap frequency, after the preparation of degenerate Fermi gases with different spin components at the temperature ~ 100 nK. V(t), the trap depth of ODT is increased exponentially from the initial V_i to the final trap depth V_f in $t_f = 60ms$ with a time constant $\tau = 12ms$ as follows,

$$V(t) = ae^{t/\tau} + b \tag{4}$$

Where $a = (V_f - V_i)/(e^{t_f/\tau} - 1)$ and $b = V_i - a$. We have experimentally tested that T/T_F values of both non-interacting gases (N = 1) and weakly interacting gases

(N=6) are conserved during the ODT is ramped up as shown in Fig. M3.

Proof of the contact relation between C and C_0 Different from the original approach using the inverse Abel transform to get 3D normalized distribution $n_{3D}^{\sigma}(k)$ from 2D TOF image [23], the method in this letter is more robust against noise because the contact is directly extracted based on the radial averaged atomic distribution $n^{\sigma}(k)$ from 2D TOF image, illustrated in Fig.2a. We calculate a term $S = 2/\pi \cdot k^3 n^{\sigma}(k)$ as a function of momentum k. The value of contact is experimentally extracted from the end tail of S profile. The contact C is therefore defined as $\mathcal{C}=\lim_{k\to\infty}\mathcal{S},$ which is slightly different from the original definition C_0 [7, 8], which stands for the total contact of the single spin state. Contact defined here is naturally normalized by atom number per spin state N_0 and wave number k_F , and is associated with \mathcal{C}_0 as $\mathcal{C} = \mathcal{C}_0/((2\pi)^3 N_0 k_F)$. Here is the detail of the proof. In a spherical symmetry system which is confirmed experimentally, we start the derivation from the original definition of the contact C_0 [7, 8],

$$C_0 = (2\pi)^3 N_0 k_F \lim_{k_{3D} \to \infty} k_{3D}^4 n_{3D}^{\sigma}(k_{3D})$$
 (5)

Where 3D wave vector k_{3D} is normalized by k_F and 3D density $n_{3D}^{\sigma}(k_{3D})$ is normalized such that $\int n_{3D}^{\sigma}(k_{3D})d^3k_{3D} = 1$. The contact C defined in this letter is written as,

$$C = \lim_{k \to \infty} S$$

$$= \lim_{k \to \infty} 2/\pi \cdot k^3 n^{\sigma}(k)$$

$$= 2/\pi \lim_{k \to \infty} k^3 \int_{-\infty}^{\infty} n_{3D}^{\sigma}(k_{3D}) dk_z$$
(6)

Here, we substitute the radial averaged atomic density with $n^{\sigma}(k) = \int_{-\infty}^{\infty} n_{3D}^{\sigma}(k_{3D}) dk_z$. From Eq(5), for large k_{3D} , the 3D atomic density can be expressed as $n_{3D}^{\sigma} = C_0/((2\pi)^3 N_0 k_F) \cdot k_{3D}^{-4} + \mathcal{O}(k_{3D}^{-5})$, in which $\mathcal{O}(k_{3D}^{-5})$ is the higher order term. Substitute n_{3D}^{σ} into Eq(6), with wave vector relation $k_{3D}^2 = k^2 + k_z^2$,

$$C = \frac{2C_0}{\pi (2\pi)^3 N_0 k_F} \lim_{k \to \infty} k^3 \int_{-\infty}^{\infty} \frac{dk_z}{(k^2 + k_z^2)^2}$$

$$= \frac{C_0}{(2\pi)^3 N_0 k_F}$$
(7)

Theoretical model of contacts of SU(N) fermions In the grand-canonical ensemble, the thermodynamic potential Ω for SU(N) fermions can be Tayler-expanded in powers of small fugacity z (virial expansion),

$$\Omega = -k_B T Q(T) [Nz + Nb_2^{\text{ni}} z^2 + \frac{N(N-1)}{2} b_2(T, a_s) z^2 + \dots],$$
(8)

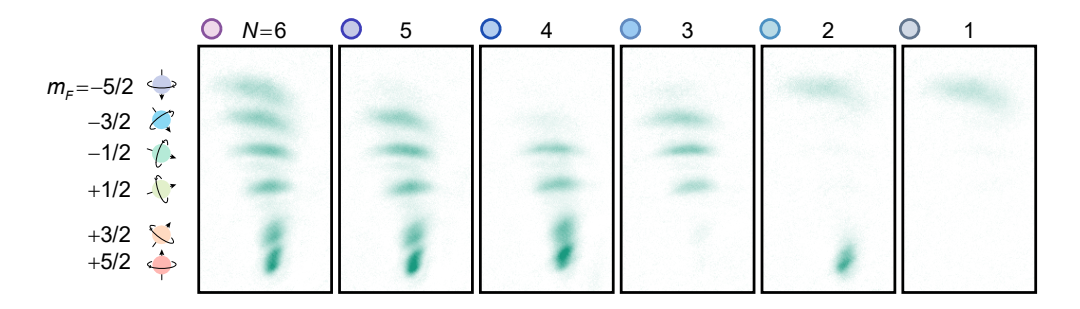


Figure M1: Fermi gases with tunable spin components. Unwanted spin components are removed by short pulses of resonant σ^+ and σ^- atomic transitions from ${}^1S_0 \rightarrow {}^3P_1$ in an around 13.6 G magnetic field. From left to right, the number of spin is prepared from N=6 to N=1. Optical Stern-Gerlach effect is used to monitor the spin configurations and split sub-clouds from top to bottom are $m_F=-5/2$ to $m_F=5/2$.

where Q(T) is the single particle partition function, b_1^{ni} is the intraspecies second order virial coefficient which purely rise from particle statistics, and b_2 is the interspecies second order virial coefficient which typically depends on the scattering length and temperature. Using the adiabatic relation [8],

$$\left[\frac{\partial\Omega}{-a_s^{-1}}\right]_{T,\mu} = \frac{\hbar^2 N}{8\pi m} \mathcal{C}_0,\tag{9}$$

we obtain an virial expansion of the contact from Ref. [29],

$$C_0 = k_B T \frac{4\pi m}{\hbar^2} Q(T) z^2 \frac{\partial b_2(T, a_s)}{\partial a_s^{-1}} (N - 1).$$
 (10)

Comparing the Taylor expansion of the grand canonical potential Ω with the virial coefficient, we obtain

$$b_2(a_s, T) = Q_2/Q,$$
 (11)

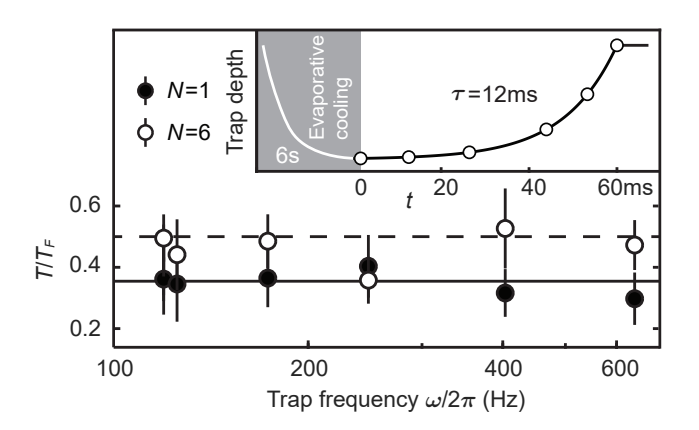


Figure M2: The ramp-up of the optical dipole trap. T/T_F of both non-interacting gases (N=1) and weakly interacting gases (N=6) are conserved during ramping up the optical dipole trap. The ODT is increased exponentially in $t_{ramp}=60$ ms with the time constant $\tau=12ms$ (inset). Gases with N=1 and N=6 components are initially prepared at $T=0.35T_F$ and $0.5T_F$, respectively.

where Q_2 is the partition function of two particles of different species in the anisotropic trap. According to Ref. [30], one could transform the problem, to a very good approximation at high temperature, to a spherical harmonic trap with trapping frequency $\tilde{\omega}$ satisfies

$$3\tilde{\omega}^2 = \omega_x^2 + \omega_y^2 + \omega_z^2. \tag{12}$$

Using the energy spectrum of two particles under isotropic harmonic confinement at arbitary scattering length obtained from solutions in Ref. [31] we can numerically determine the partition function as well as the derivative with respect to a_s^{-1} .

According to local density approximation, the virial coefficient for the trapped system can be related to that of the homogeneous system.

$$b_2 = b_2^{homo}/2^{3/2},\tag{13}$$

$$Q \approx (k_B T / \hbar \bar{\omega})^3, \tag{14}$$

where $\bar{\omega}^3 = \omega_x \omega_y \omega_z$. From Ref. [32], one obtain $b_2^{homo} = -2a_s/\lambda$, where λ is the thermal de Broglie length. Com-

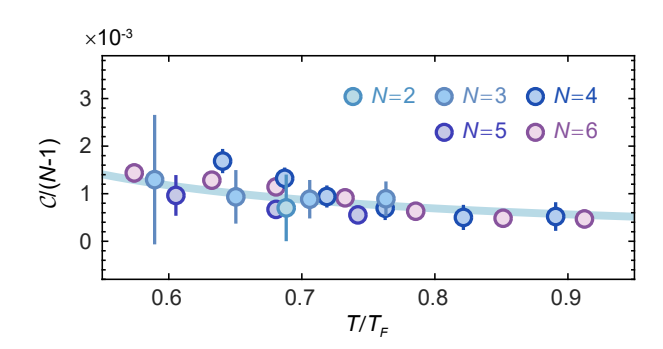


Figure M3: Scaled contact vs temperature Contact of different SU(N) gases are scaled on the N=2 components case by $\mathcal{C}/(N-1)$. The solid curve is the theoretical simulation multiplied by a factor of 6.5.

bining the equations above, under LDA, we obtain

$$C_0 = k_B T \frac{4\pi m}{\hbar^2} (k_B T / \hbar \bar{\omega})^3 z^2 \frac{2a_s^2}{2^{3/2} \lambda} (N - 1).$$
 (15)

In the high temperature limit, $z = NN_0(\hbar \bar{\omega}/k_B T)^3$. The total contact of SU(N) fermions is then written as

$$C_{SU(N)} = NC_0 = N_0^2 N(N-1) \frac{2\sqrt{2}\pi m}{\hbar^2} \frac{(\hbar\bar{\omega})^3}{(k_B T)^2} \frac{a_s^2}{\lambda}.$$
 (16)

Contact of single component Bose gas Applying the virial expansion to a single-component Bose gas, the thermodynamic potential Ω_B at high temperatures is written as

$$\Omega_{\rm B} = -k_B T Q(T) [z + b_2^{\rm ni} z^2 + b_2(T, a_s) z^2 + \dots].$$
(17)

Here b_2 is the second order virial coefficient for two distinguishable particles, i.e., the same as that for the intraspecies b_2 for SU(N) fermions, and b_2^{ni} is a term that accounts for bosonic statistics which is independent of the scattering length. Using the adiabatic relation [8],

$$\left[\frac{\partial\Omega_B}{-a_s^{-1}}\right]_{T,\mu} = \frac{\hbar^2}{8\pi m}C_B,\tag{18}$$

we obtain an virial expansion of the contact,

$$C_{\rm B} = k_B T \frac{8\pi m}{\hbar^2} Q(T) z^2 \frac{\partial b_2(T, a_s)}{\partial a_s^{-1}}.$$
 (19)

Using $z = NN_0(\hbar \bar{\omega}/k_B T)^3$, we obtain

$$C_{\rm B} = (N_0 N)^2 \frac{2\sqrt{2}\pi m}{\hbar^2} \frac{(\hbar \bar{\omega})^3}{(k_B T)^2} \frac{a_s^2}{\lambda}.$$
 (20)

Compare \mathcal{C}_{B} and $\mathcal{C}_{\mathrm{SU(N)}}$, we obtain

$$C_{SU(N)} = \frac{N-1}{N}C_{B}.$$
 (21)

In the limit $N \to \infty$, $\mathcal{C}_{SU(N)}$ approaches \mathcal{C}_B with a scaling of 1/N.

Acknowledgement G.-B. J. acknowledges the generous support from the Hong Kong Research Grants Council and the Croucher Foundation through GRF16311516, and GRF16305317, GRF16304918, GRF16306119, C6005-17G and the Croucher Innovation grants respectively. Q. Z. is supported by NSF PHY 1806796.

Competing interests. The authors declare that they have no competing interests.

Data availability. The data that support the findings of this study are available from the corresponding authors upon reasonable request.